Trees (2003) 17:23–30
DOI 10.1007/s00468-002-0202-6

ORIGINAL ARTICLE

Thierry Fourcaud · Patrick Lac

Numerical modelling of shape regulation and growth stresses in trees

I. An incremental static finite element formulation

Received: 30 October 2001 / Accepted: 4 July 2002 / Published online: 14 September 2002

Abstract This paper is the first of a series focusing on the biomechanical analysis of live trees. The finite element method (fem) is the most common method used for the analysis of complex mechanical structures. Several fem industrial codes exist, but they need to be adapted to calculate the mechanical behaviour of growing trees. A general incremental model has been developed for this specific application. In this model, time was discretised and for any developmental stage, a new equilibrium was written considering the increment of weight due to the mass of new wood layers and new vegetative elements being added. Maturation strains of new-formed cells were also considered for the simulation of the shoot reorientation process. This model was intended for use at the whole plant level. A multi-layer beam finite element is presented, which is well adapted to discretise tree limbs. The shape evolution of the structure was represented at each time step by the nodal displacement vector. The mechanical stresses induced as a result of growth were determined within the stem using a cumulative process taking into account the past history of each growth ring. The first basic results of growth stresses and shape evolution were compared with already published results at the branch level.

Keywords Trees · Biomechanics · Growing structure · Finite element method · Multi-layer beam element

Introduction

The stem and branches of trees undergo internal stresses which are due to two types of actions: the self-weight of the structure, which mainly results in compression forces and bending or torsion moments, and internal growth stresses which originate in xylem during cell lignification (Archer 1986). In both cases, the development of internal stresses and the deformation of tree limbs must be considered as a cumulative process and account for growth and architectural patterns of the plant, as well as its loading history. In the past, several analytical models have been developed in order to calculate growth stresses at a local level in the stem (Kubler 1959; Gillis 1973; Archer 1986; Fournier et al. 1990). These studies found a technological interest that has mainly focused on the splitting or twisting of planks. Studies on the analysis of the movement of growing branches submitted to self-weight have also been carried out (Ford 1985; Cannell et al. 1988; Castéra and Morlier 1991; Alméras et al. 2002). The main goal of these studies is to determine if a relationship exists between geometry and weight of axes, so that the deflection of the structure remains within allowable loading limits. However, when the stresses and shape of a structure are calculated as cumulative processes, this concept should be valid at any stage of development. Some interesting studies have considered these two mechanical aspects at the same time, i.e. bending of the stem under incremental loads as well as reorientation due to non-axisymmetric maturation strains (Wilson and Archer 1974; Fournier et al. 1994). This last approach has been maintained in this current paper in order to analyse numerically the relationships between the swaying movement of the stem and the heterogeneity of the inner wood structure, e.g. occurrence of reaction wood and cumulated growth stresses. The finite element method (fem) is the most common numerical method used in solid mechanics to determine the stress, strain and displacement fields in an equilibrated domain (Zienkiewicz and Taylor 1998). However, fem industrial software is not adapted to calculate the mechanical behaviour of live trees. Instead, a general incremental finite element formulation has been developed. This model took into consideration the progressive volume extension due to growth, as well as the resulting incremental biomechani-

T. Fourcaud (✉) · P. Lac
Laboratoire de Rhéologie du Bois de Bordeaux,
UMR 5103 CNRS/INRA/University of Bordeaux I,
Bordeaux, France
e-mail: fourcaud@lrbb3.pierroton.inra.fr
Fax: +33-5-56680713

T. Fourcaud
Programme Modélisation des Plantes, AMAP, CIRAD-AMIS,
France

cal behaviour, i.e. superposition of stresses and strains, deformation of the structure and biomechanical response to gravitropism (Timell 1986). In a new and original approach this model has been applied at the whole tree level rather than at the plant organ level (Mattheck and Kubler 1995). For this purpose, the description of a Bernoulli 3D multi-layer beam element is presented. The geometry of such an element is appropriate to describe tapered structures. The multi-layer model is also a natural choice with regards to the radial variation of wood properties that results from the growth of the cross-section. Simple applications of the model have been run. Growth stress calculations have been compared to the Kubler (1959) analytical formulation in the case of a cylinder that was submitted to axisymmetrical maturation strains. Shape evolution of a single growing branch is shown and discussed. The application to branching structures will be presented in a subsequent paper.

Materials and methods

Model development, general incremental formulation

In solid mechanics, the calculation of stresses, strains and displacements by fem is carried out by discretising the displacement field. This discretised field is substituted into the expression of the virtual work principle (VWP) (Zienkiewicz and Taylor 1998). Discretisation is obtained choosing control points or nodes in the domain and writing the displacement field under the form

$$U = Nq \tag{1}$$

in which U is the column vector which contains the three displacement components U_x, U_y and U_z with regards to the global referential axis; q is the column vector containing all the unknown nodal displacements. Matrix N contains shape functions depending on spatial co-ordinates. Usually, these functions are polynomials, the degree of which depends on the number of nodes.

The strain field can then be expressed as

$$\varepsilon = Bq \tag{2}$$

The strain shape function matrix B is inferred from N by derivation according to strain-displacement relations.

A growing tree is a domain that is evolving. For numerical calculation, the time variable has to be discretised. At any time t_n that the equilibrium of the domain Ω_n is reached, the equations to be satisfied are written in the standard form of VWP

$$\int_{\Omega_n} B^T \sigma_n d\Omega = f_n \tag{3}$$

B^T is the transpose of matrix B. σ_n is the column vector of the stress field components; f_n is the vector of nodal external loads applied on Ω_n at time f_n. This vector can contain concentrated loads, e.g. fruit or leaf weight, as well as equivalent nodal forces due to distributed loads such as self-weight or prevailing wind loading.

After a period of time $\Delta t_n = t_{n+1} - t_n$ when growth has occurred, the structure has occupied the new domain Ω_{n+1} which can be expressed by

$$\Omega_{n+1} = \hat{\Omega}_n + \Delta\Omega_n \tag{4}$$

$\hat{\Omega}_n$ corresponds to the domain Ω_n which has been deformed under the applied loads during Δt_n. $\Delta\Omega_n$ is the new volume of material resulting from the growth at the periphery of Ω_n.

The new equilibrium at time t_{n+1} is naturally written as

$$\int_{\Omega_{n+1}} B^T \sigma_{n+1} d\Omega = f_{n+1} \tag{5}$$

In order to simplify the demonstration, the strain shape function matrix B used in Eq. 3 has been extended to the new domain $\Delta\Omega_n$. Rigorously, nodes have to be added in $\Delta\Omega_n$ and strain shape functions have to be recalculated. In both cases, strains are continuous at the interface of the two domains Ω_n and $\Delta\Omega_n$.

The fem incremental formulation, representing the new equilibrium reached during the period of time Δt_n, results from the difference (Eq. 5)–(Eq. 3) with regards to Eq. 4. Assuming that the deformed domain is very close to the initial domain $\hat{\Omega}_n \simeq \Omega_n$, this incremental formulation can be written as

$$\int_{\Omega_n} B^T (\sigma_{n+1} - \sigma_n) d\Omega + \int_{\Delta\Omega_n} B^T \sigma_{n+1} d\Omega = f_{n+1} - f_n \tag{6}$$

Let $\sigma_{n+1} - \sigma_n = \Delta\sigma_n$ and $f_{n+1} - f_n = \Delta f_n$. As the part $\Delta\Omega_n$ did not exist before time t_{n+1}, it can be considered that $\sigma_n = 0$ in $\Delta\Omega_n$, i.e. $\sigma_{n+1} = \Delta\sigma_n$ in $\Delta\Omega_n$. Finally, the finite element formulation of the equilibrium equations, which must be satisfied during the time increment Δt_n is given in the incremental form:

$$\int_{\Omega_n} B^T \Delta\sigma_n d\Omega + \int_{\Delta\Omega_n} B^T \Delta\sigma_n d\Omega = \Delta f_n \tag{7}$$

This equation only concerns the equilibrium of the incremental loading that is applied on the whole structure during the period Δt_n. Compared to the classical incremental formulation used for time dependent problems (Owen and Hinton 1980), the presence of the second term in the left-hand member, which refers to the equilibrium of the new domain $\Delta\Omega_n$ should be noted.

Equation 7 can now be written in terms of nodal displacements. According to Eq. 2, the strain increment is expressed as

$$\Delta\varepsilon_n = B\Delta q_n \tag{8}$$

The strain $\Delta\varepsilon_n$ can be separated into elastic $\Delta\varepsilon_n^{el}$ and maturation $\Delta\varepsilon_n^{MS}$ strains as

$$\Delta\varepsilon_n = \Delta\varepsilon_n^{el} + \Delta\varepsilon_n^{MS} \tag{9}$$

Maturation strains (MS) refer to the volume changing of new wood cells during differentiation and maturation process. MS increment $\Delta\varepsilon_n^{MS}$ occurring in a time interval $\Delta t_n = t_{n+1} - t_n$ is defined by:

$$\begin{aligned} \Delta\varepsilon_n^{MS} &= \alpha_n \quad \text{in the domain } \Delta\Omega_n \\ \Delta\varepsilon_n^{MS} &= 0 \quad \text{in the domain } \Omega_n \end{aligned} \tag{10}$$

Using Eq. 9 and Eq. 10, the constitutive equation is written in incremental form

$$\begin{aligned} \Delta\sigma_n &= D\Delta\varepsilon_n - D\alpha_n \quad \text{in domain } \Delta\Omega_n \\ \Delta\sigma_n &= D\Delta\varepsilon_n \quad \text{in domain } \Omega_n \end{aligned} \tag{11}$$

denoting D the material stiffness matrix at the current material point. As D could be time dependent, an index n has to be added to the term.

Substituting from Eq. 8 the strain increment in Eq. 11, incremental form Eq. 7 is resumed to the linear system

$$K_n \Delta q_n = \Delta F_n \tag{12}$$

K_n is the stiffness matrix that is used to calculate the equilibrium of domain Ω_{n+1}, ΔF_n is the sum of both the nodal vector of external static load increment Δf_n, and the nodal load vector $\Delta\Lambda_n$ issuing from MS:

$$\Delta\Lambda_n = \int_{\Delta\Omega_n} B^T D\alpha_n d\Omega \tag{13}$$

The $\Delta\varepsilon_n$ continuity assumption at the interface of the two domains Ω_n and $\Delta\Omega_n$ allows the MS restraint by the internal core Ω_n to be taken into consideration. This restraint induces displacements. The load vector Eq. 13 creates the same increment of node displacements as the MS.

The matrix K_n is given by

$$K_n = \int_{\Omega_n} B^T DBd\Omega + \int_{\Delta\Omega_n} B^T DBd\Omega \tag{14}$$

Finally, at each period of time Δt_n, we get:

1. The displacement increment Δq_n, solving the system given by Eq. 12
2. The strain increment $\Delta \varepsilon_n$ substituting Δq_n back into Eq. 8
3. The stress increment $\Delta \sigma_n$ from Eq. 11.

The growth stresses occurring in the domain Ω_{n+1} are calculated using the recurrence formula:

$$\sigma_{n+1} = \sigma_n + \Delta\sigma_n \tag{15}$$

During the total period of growth (t_0, t_N), the incremental process which is described above is repeated N times. Due to the cumulative process (Eq. 15), stresses at time t_N could be written as

$$\sigma_N = \sum_{n=0}^{N-1} \Delta\sigma_n \tag{16}$$

Nevertheless, considering new layers $\Delta\Omega_p(P{=}0, N{-}1)$ appear successively, it is necessary to take into consideration the date t_p when $\Delta\Omega_p$ has been made. Let $\Delta\sigma_n^p$ be the stress increment calculated during the period of time Δt_n in the domain $\Delta\Omega_p$, the total stresses in this domain at t_N results from the addition of $N–p$ increments according to the formula

$$\sigma_N^p = \sum_{n=p}^{N-1} \Delta\sigma_n^p \tag{17}$$

Regarding to this cumulative formula, it appears that the growth stress field in a layer $\Delta\Omega_p$ depends on the age of this layer, i.e. the older the layer, the more increments that have been cumulated. Eq. 17 is a time discretised formulation of growth stresses which is useful for numerical calculations. The continuous analytical expression was first described by Kubler (1959) for axisymmetric growth. This was used to validate the finite element approach that is presented here.

Finite element calculation of a complex structure requires the geometrical domain to be discretised with simple shape elements (mesh). The discretisation of the displacement vector U (Eq. 1) is written at the element level, i.e. the shape functions are calculated on each element e. Element e is associated with an elementary stiffness matrix which can be written like Eq. 14 in the form

$$k_n^e = \int_{\Omega_n^e} (B^e)^T D^e B^e d\Omega + \int_{\Delta\Omega_n^e} (B^e)^T D^e B^e d\Omega \tag{18}$$

The global stiffness matrix K_n comes from the assembly of elementary stiffness matrices k_n^e. This assembly phase is described by Zienkiewicz and Taylor (1998). Calculation of vector ΔF_n is performed in the same way using the two elementary nodal load vectors $\Delta\Lambda_n^e$ and Δf_n^e. The next paragraph shows the calculation of these elementary vectors in the case of using beam elements.

Modelling growth with beam elements

Slender branch shape results from growth speed differences between radial and axial directions. Beam theory which is based on decoupling between the axial direction x and the (y, z) transverse plane (cf. Appendix), is particularly well adapted to model structures composed of elongated limbs. The above general incremental theory has been developed for a multilayer 3D straight Bernoulli beam element.

The strain/displacement relations (Eqs. 2, 8) are defined considering the decomposition $B^e{=}G(y, z)b^e(x)$ where matrices G and b^e are given in the Appendix (Eqs. 33, 35). Beam element e is described by its constant length L^e and its cross-section area S_n^e. Secondary growth is taken into account extending matrix G to the new peripheral layer ΔS_n^e. The elementary stiffness matrix (Eq. 18) then becomes

$$k_n^e = \int_{L^e} \int_{S_n^e + \Delta S_n^e} (B^e)^T D^e B^e d\Omega \tag{19}$$

This extension induces the cross-section area $S_n^e + \Delta S_n^e$ remains plane during Δt_n. This modelling is a simple way to take into account the restriction of MS by the internal core S_n^e.

Growth in length requires new elements to be added to the stem extremity, involving all the elements that did not have the same age at a fixed time. Denoting $t_{p(e)}$ the date of creation of element e, the total cross section area results from the addition of $n–p(e)$ layers according to the formula

$$S_n^e = \sum_{j=p(e)}^{n-1} \Delta S_j^e \tag{20}$$

Substituting Eq. 20 in Eq. 19 and using the factorised expression of B^e allows the elementary stiffness matrix to be calculated as

$$k_n^e = \int_{L^e} (b^e)^T \left[\sum_{j=p(e)}^{n} \int_{\Delta S_j^e} G^T D_j^e G dS \right] b^e dx \tag{21}$$

where D_j^e is the 3×3 diagonal material stiffness matrix in the layer which appears at t_j in element e. The term between the square bracket is the 4×4 multi-layer beam stiffness matrix. It depends on the cross-section shape and it can be calculated explicitly for simple forms or by a numerical integration scheme.

If self-weight is the only external force considered, the vector of nodal load increment applied at t_n on element e is expressed using an incremental form of Eqs.39 and 40.

$$\Delta f_n^e = \int_{L^e} (N^e)^T \Delta p_n^e dx_n^e \tag{22}$$

where Δf_n^e is the vector of concentrated loads at nodes and Δp_n^e the vector of distributed loads defined by

$$\Delta p_n^e = \left(\int_{\Delta S_n^e} P_x^e dS \quad \int_{\Delta S_n^e} P_y^e dS \quad \int_{\Delta S_n^e} P_z^e dS \quad 0 \right)^T \tag{23}$$

Substituting Eq. 37 in Eq. 13 gives the nodal load vector issuing from MS:

$$\Delta\Lambda_n^e = \int_{L^e} (b^e)^T \left[\int_{\Delta S_n^e} G^T D_n^e \alpha_n^e dS \right] dx \tag{24}$$

The term between the square brackets is the 4×1 vector of forces and moments cinematically equivalent to the restrained MS. The calculation of this vector is governed by the choice of models describing the cross-section shape ΔS_n^e and the vector of MS α_n^e. Samples will be shown in a second part of this series of papers. For instance, it is easy to show that axisymmetric models for both ΔS_n^e and α_n^e do not induce bending moments nor torsion moment, but only axial load.

Results and discussion

Growth stresses in an axisymmetric case

A very simple case of growing cylindrical solid has been considered in order to evaluate the model of growth stress calculation (Eqs. 7–17). The domain grows in the radial direction, reaching radius R at time T. Length L was fixed. The material was assumed to be elastic, isotropic and homogeneous, with constant longitudinal Young's modulus E. Self weight has been neglected here in order to focus on stresses due to MS. New layers were submitted to constant and homogeneous axisymmetric longitudinal MS α_0. In this example cross-sections were supposed to move in the longitudinal direction without distortion. The longitudinal displacement component U_x then depends on the single longitudinal variable x. Two

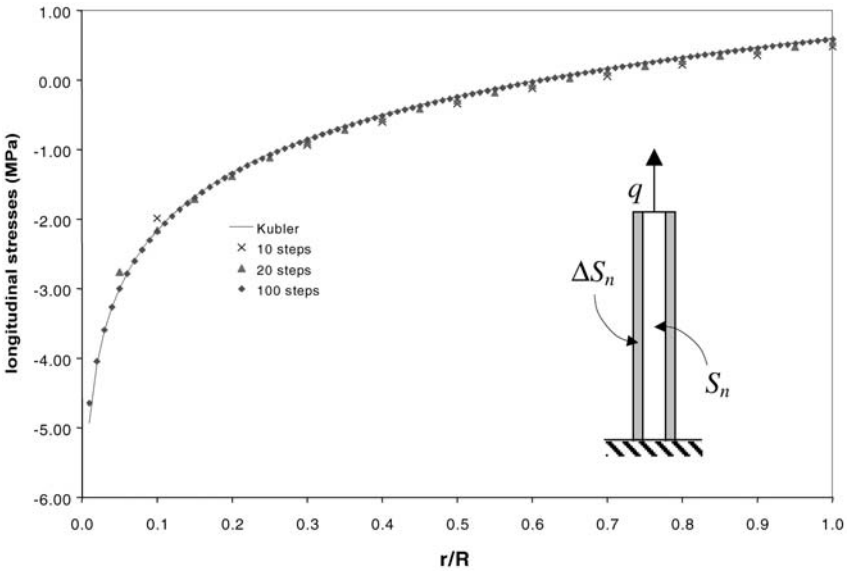

Fig. 1 Comparison of growth stress calculation with Kubler's analytical model (1959) for 10, 20 and 100 steps of calculation

nodes are sufficient to discretise the problem. One node was clamped and the displacement U_x of the other one was denoted q as presented in Fig. 1. According to Eq. 1, the displacement field U_x was linearly interpolated on interval [0, q] as $U_x = \frac{x}{L}q$. Matrices B and D were reduced to scales: B=1/L and D=E.

During the period of growth [t_0=0, t_N=T], N steps of calculation have been considered. Let ΔS_n be the layer cross section area which has been formed during the period $\Delta t_n = t_{n+1} - t_n$ and S_n the inner cross section area of the domain that already existed at the beginning of the step. The new equilibrium at this stage was given by the linear system $K_n \Delta q_n = \Delta \Lambda_n$. The global stiffness matrix was calculated using Eq. 14: $K_n = \frac{E}{L}(S_n + \Delta S_n)$. Nodal axial load due to MS was given by Eq. 13 : $\Delta \Lambda_n = E\alpha_0 \Delta S_n$.

The n+1th displacement increment of the top node was then $\Delta q_n = \frac{\alpha_0 L \Delta S_n}{(S_n + \Delta S_n)}$. At any point in the layer $\Delta\Omega_p$, which appeared at t_p, growth stresses were calculated at time T with regards to Eq. 8, Eq. 11 and Eq. 17:

$$\sigma_N^p = E\alpha_0 \left(\sum_{n=p}^{N-1} \frac{\Delta S_n}{S_n + \Delta S_n} - 1 \right) \tag{25}$$

The famous continuous analytical expression $\sigma(r) = -E\alpha_0(1+2\ln r/R)$ of accumulated growth stresses given by Kubler (1959) can be easily deduced from Eq. 25 by tending the step number N towards infinity. When the incremental cross-section area is small enough, it can be neglected at the denominator and approximated at the numerator as $\Delta S_n \approx 2\pi r_n \Delta r_n$ where $\Delta r_n = \frac{R}{N}$. At the limit, the sum is substituted by an integral in Eq. 25. It becomes

$$\sigma_n^p \xrightarrow{N \to \infty} E\alpha_0 \left(\int_{r_p}^{R} 2\frac{dr}{r} - 1 \right)$$

where r_p is the external radius of the cylinder at time t_p. Calculation of this integral gives the Kubler's formula for r=r_p.

The model has been run considering N=10, 20 and 100 steps of calculation (rings) to reach radius R. Results are presented in Fig. 1 taking the following characteristics: α_0=–200 μdef, E=3,000 MPa.

Branch shape simulation

Our finite element model has been applied to calculate the shape evolution of a non-ramified growing branch. At each period of time Δt_n, both primary lengthening and radial extension were considered. A series of multi-layer cylinders have been used to approximate tree branch geometry (Fig. 2). Each new length increment has been represented by a new cylinder. Each new ring appearing at the branch periphery has been represented by a new layer on the existing cylinders. The branch was submitted to the corresponding increment of weight. As they were considered thin enough, i.e. with a small diameter/length ratio, the cylinders were modelled using Bernoulli 3D beam elements (cf. Appendix). For each step $n \subset [0, N-1]$, global stiffness matrix K_n was assembled using the expression of k_n^e given in Eq. 21. In the same way, assembly of the nodal incremental load vector ΔF_n was performed using elementary vectors Δf_n^e given in Eq. 22. Maturation strains did not have been considered, i.e. $\Delta \Lambda_n^e = 0$ for all elements. Additional concentrated loading has also been taken into consideration when the branch was supposed to bear needles. At each step of calculation, the displacement increment Δq_n was obtained solving Eq. 12. The branch geometry was updated at the end of the step calculating the new node co-ordinates of elements. The following growth was applied to the deformed shape.

The following numerical inputs were chosen according to averaged measured data of maritime pine trees (*Pinus pinaster* Ait.). The branch initial leaning angle is 50° from vertical. At any step, the length of new ele-

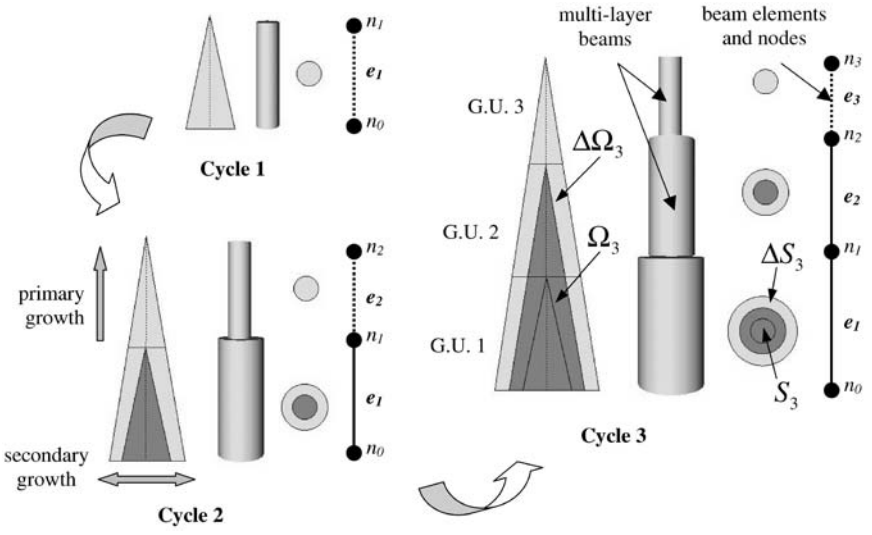

Fig. 2 Geometrical representation of a tree axis. At each cycle of growth, a new layer of matter $\Delta\Omega_n$ appears on the existing structure Ω_n. The axis geometry has been approximated by a series of multi-layer cylinders. According to this representation, the structure was discretised with beam elements e_i that were connected to each other by nodes n_i. Growth in length (primary growth) needed to have one or more new elements introduced at the top end whereas cross-section extension (secondary growth) was taken into account by adding a new cross-section area ΔS_n at the element periphery

Table 1 Time evolution of growth unit radius (mm) of simulated branch

Growth Unit number																				
	20	0.20																		
	19	0.20	0.66																	
	18	0.20	0.64	0.89																
	17	0.20	0.62	0.86	1.07															
	16	0.20	0.60	0.83	1.03	1.21														
	15	0.20	0.57	0.80	0.99	1.16	1.32													
	14	0.20	0.56	0.77	0.95	1.12	1.27	1.42												
	13	0.20	0.53	0.74	0.91	1.07	1.22	1.36	1.50											
	12	0.20	0.52	0.71	0.88	1.03	1.17	1.31	1.44	1.57										
	11	0.20	0.50	0.69	0.85	0.99	1.13	1.26	1.39	1.51	1.64									
	10	0.20	0.49	0.67	0.82	0.96	1.09	1.21	1.34	1.46	1.58	1.70								
	9	0.20	0.48	0.65	0.80	0.93	1.05	1.17	1.29	1.41	1.52	1.64	1.75							
	8	0.20	0.46	0.63	0.77	0.90	1.02	1.13	1.24	1.35	1.46	1.58	1.69	1.80						
	7	0.20	0.45	0.61	0.75	0.87	0.98	1.09	1.20	1.30	1.41	1.52	1.63	1.73	1.85					
	6	0.20	0.43	0.59	0.72	0.84	0.95	1.06	1.16	1.26	1.36	1.46	1.57	1.67	1.78	1.88				
	5	0.20	0.42	0.57	0.69	0.81	0.92	1.02	1.12	1.22	1.31	1.41	1.51	1.61	1.71	1.81	1.92			
	4	0.20	0.39	0.53	0.66	0.77	0.87	0.97	1.07	1.17	1.26	1.35	1.45	1.54	1.64	1.74	1.84	1.95		
	3	0.20	0.40	0.52	0.64	0.74	0.84	0.94	1.03	1.13	1.22	1.31	1.40	1.49	1.58	1.68	1.78	1.88	1.98	
	2	0.20	0.35	0.49	0.59	0.70	0.80	0.89	0.98	1.07	1.16	1.25	1.34	1.42	1.52	1.61	1.70	1.80	1.90	2.00
	1	0.20	0.35	0.45	0.57	0.66	0.75	0.84	0.93	1.02	1.11	1.20	1.28	1.37	1.45	1.54	1.63	1.73	1.82	1.92	2.02
		1	2	3	4	5	6	7	8	9	10	11	12	13	14	15	16	17	18	19	20
	Step number																			

ments, which correspond to the new growth units (GU) appearing at the branch top, is fixed to 25 cm. The evolution of element radius during the simulation is given in Table 1. Wood material is considered homogeneous and isotropic. The longitudinal Young's modulus is fixed to 3,000 MPa. The distributed load density P_y is taken as 1 g.cm^{-3}. Two strategies of primary growth have been tested. The first one assumed that the new element that appeared at any stage n was oriented in the direction of the bearing element (Fig. 3a). The second strategy assumed that the new element was connected with a fixed global orientation of 50° from vertical (Fig. 3b). This last example has been also simulated taking into account additional loading due to the existence of needles (Fig. 3b'). Each group of needles weighed 20 g and it was supposed to stay on the branch during five complete steps (needle life span). Global vector of concentrated load increment has been applied according to scheme Fig. 4. To be rigorous, two calculations per step would be performed in order to take into account the appearance and disappearance of total leaf weight for deciduous leaves. We performed only one calculation per step.

Numerical results of simulated branch shape evolution (Fig. 3) are given in Table 2 for the three samples. It is clear that branch form is highly sensitive to the distribution of needle biomass as well as the orientation of new vegetative elements that appear at the branch tip. Similar calculations using a finite difference method have been performed by Castéra and Morlier (1991), considering more complex and realistic loadings. However, resulting branch shapes are comparable to those shown in the present paper.

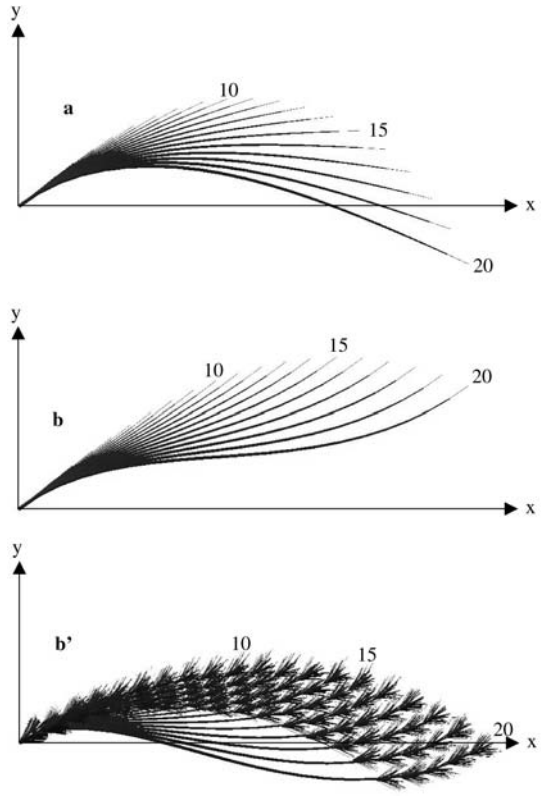

Fig. 3a, b Stepwise evolution of branch shape during growth simulation under self weight loading. **a** Apical growth occurred in the direction of the bearing element; **b** apical growth occurred in a fixed global direction; **b'** addition of concentrated loads due to needles

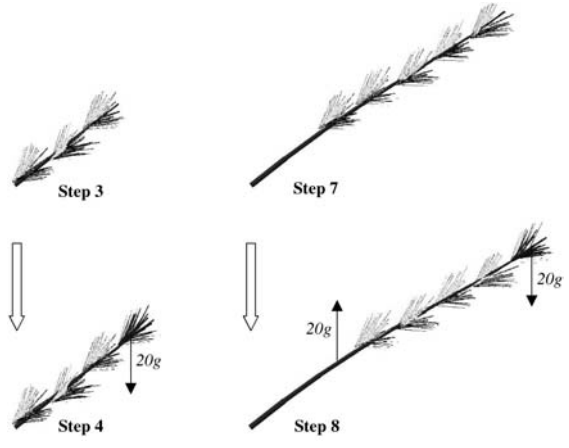

Fig. 4 Application of concentrated load increment corresponding to needle weight. A weight increment was applied when new group of needles appeared at the top branch. The weight of needles older than 5 years was removed

Conclusion

The study of plant biomechanics is used to investigate the relationship between the growth and the mechanical behaviour of plants under internal or external loading. For this purpose, an incremental finite element formulation of a linear elasticity problem has been presented. The originality of this model is its adaptation to growing structures, i.e. domains with time dependent volume. The time is discretised in periods during which a new layer of matter is added on the external surface of the volume. Load increments – which can originate both from weight increment, maturation strains in the new domain and other external forces – are applied on the new whole domain. The general fem formulation, which is given in this paper, can be used to investigate classical problems such as calculation of growth stress distribution in a piece of wood (Kubler 1959; Archer 1986). Growth stresses calculated with this formulation were in coherence with the Kubler analytical model in the axisymmetric case. Shape evolution of a growing branch (Archer and Wilson 1970; Castéra and Morlier 1991; Fournier et al. 1994) can also be investigated with this numerical approach. However, the most original application is at the tree level. This provides an interesting numerical way to supply physiological functions and mechanical support (Niklas and O'Rourke 1982; Morgan and Cannell 1988) considering the whole branching system. For this purpose, a 3D multi-layer beam element has been proposed. This element integrates the radial extension and cumulative stress processes. The model has been applied to very simple examples at the stem or branch level. Realistic shapes have been obtained in accordance with the literature. This general method could be implemented in existing plant architecture simulation software. This is the subject of a subsequent paper.

Acknowledgements Thanks are due to Drs. A Stokes and N. Harries for their comments and corrections.

Appendix

In beam theory, plane sections remain plane during the deformation process and suffer no extension. The thin beam theory adds the well-known Bernoulli-Euler assumption. This consists of neglecting shear deformations due to flexion, which is equivalent to stating normals remain normal during the deformation. Using these assumptions the local displacements can be written under a form where transversal co-ordinates y and z are separated from the longitudinal co-ordinate x:

$$U_x = u_x - y\frac{du_y}{dx} - z\frac{du_z}{dx}, \quad U_y = u_y - z\omega, \quad U_z = u_z + y\omega \tag{26}$$

The generalised displacements (Fig. 5) u_x, u_y, z_u, ω, $\frac{du_y}{dx}$, $\frac{du_z}{dx}$ are functions of the single variable x.

The strains are available as

$$\varepsilon_{xx} = \varepsilon - yK_z + zK_y, \quad \gamma_{xy} = -zK_x, \quad \gamma_{xz} = yK_x \tag{27}$$

with the generalised strains, i.e. traction strain ε, flexion strains K_y and K_z, torsion strain K_x, given in terms of generalised displacements as

$$\varepsilon = \frac{du_x}{dx}, \quad K_z = \frac{d^2u_y}{dx^2}, \quad K_y = -\frac{d^2u_z}{dx^2}, \quad K_x = \frac{d\omega}{dx} \tag{28}$$

Nodes of a beam finite element are positioned on x-axis. Nodal displacements correspond to the generalised displacement values given at each node. Figure 6 shows the numbering of the nodal displacements $q_i^e, i = \{1, 12\}$ for two node beam element. Shape functions which are classically associated with a Bernoulli beam element are Lagrangian first order polynomials (L functions) and Hermitian third order polynomials (H functions).

Table 2 (X, Y) positions (cm) of element nodes at simulation steps 1, 10, 15 and 20 for branches *a* apical growth occurred in the direction of the bearing element; *b* apical growth occurred in a fixed global direction; and *b'* addition of concentrated loads due to needles

Branch a		Branch b		Branch b'	
X	Y	X	Y	X	Y
Step 1					
0.0	0.0	0.0	0.0	0.0	0.0
19.2	16.0	19.2	16.0	20.6	14.4
Step 10					
0.0	0.0	0.0	0.0	0.0	0.0
19.8	15.2	19.8	15.2	22.0	12.1
40.6	29.1	40.5	29.3	46.0	20.2
62.2	41.9	61.8	42.4	70.9	26.2
84.2	53.8	83.4	55.2	95.8	31.7
106.7	64.9	105.1	67.7	121.0	37.1
129.4	75.5	126.8	80.3	145.9	43.2
152.3	85.7	148.2	93.3	170.5	50.5
175.4	95.6	169.3	106.9	194.5	59.2
198.5	105.2	189.9	121.1	217.8	69.7
221.7	114.6	209.9	136.2	240.0	82.2
Step 15					
0.0	0.0	0.0	0.0	0.0	0.0
20.2	14.8	20.1	14.8	22.3	11.5
41.8	27.4	41.7	27.6	46.9	17.8
64.5	37.9	64.1	38.7	72.3	20.8
88.0	46.8	87.2	48.5	97.9	22.0
112.1	54.1	110.7	57.5	123.7	22.1
136.5	60.1	134.4	66.0	149.5	22.0
161.2	64.9	158.2	74.2	175.4	22.0
186.2	68.8	182.0	82.5	201.3	22.6
211.2	71.9	205.6	91.2	227.1	24.2
236.4	74.4	229.1	100.5	252.8	27.1
261.5	76.3	252.2	110.5	278.2	31.5
286.7	77.8	274.9	121.5	303.2	37.6
311.9	79.0	296.9	133.7	327.6	45.7
337.0	79.9	318.2	147.0	351.1	55.8
362.1	80.7	338.5	161.6	373.4	68.2

Branch a		Branch b		Branch b'	
X	Y	X	Y	X	Y
Step 20					
0.0	0.0	0.0	0.0	0.0	0.0
20.5	14.4	20.4	14.4	22.6	11.0
42.9	25.5	42.7	25.8	47.6	15.5
66.6	33.7	66.2	34.6	73.2	15.5
91.1	39.2	90.5	41.3	98.8	12.8
116.2	42.2	115.2	46.2	124.2	7.9
141.4	43.1	140.2	49.8	149.4	1.9
166.8	42.0	165.3	52.5	174.6	–4.9
192.0	39.2	190.6	54.5	199.7	–11.9
217.1	35.0	216.0	56.3	225.0	–18.7
242.0	29.5	241.4	58.2	250.4	–25.1
266.7	22.9	266.7	60.4	276.0	–30.5
291.1	15.4	292.1	63.2	301.8	–34.9
315.3	7.2	317.3	66.9	327.8	–37.8
339.2	–1.7	342.3	71.7	353.9	–39.0
363.0	–11.0	367.0	77.7	379.9	–38.3
386.5	–20.7	391.3	85.2	405.8	–35.5
409.8	–30.7	415.0	94.3	431.1	–30.4
433.0	–40.8	437.8	105.1	455.8	–22.9
456.0	–51.2	459.7	117.6	479.4	–13.0
478.8	–61.6	480.3	131.9	501.7	–0.7

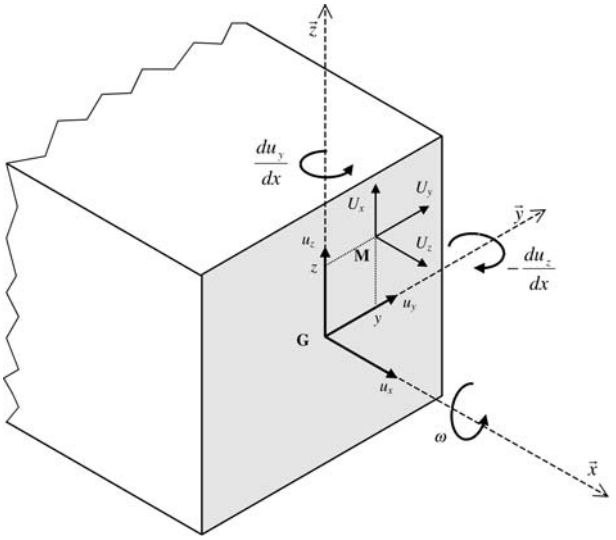

Fig. 5 In beam theory, the displacements U of any point M are defined by the six components of the generalised displacements. u_x, u_y, u_z are the displacements of point G. ω, $-\frac{du_z}{dx}$, $\frac{du_y}{dx}$ are the positive rotations of the cross-section normal $\vec{x}$. ($\vec{x}$, $\vec{y}$, $\vec{z}$) are the local directions of the beam. $\vec{x}$ is called the beam reference axis

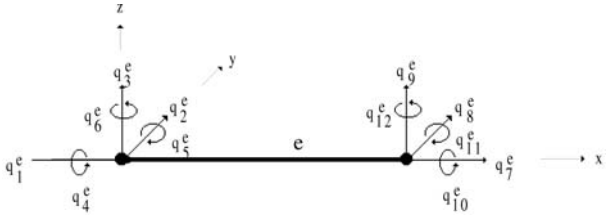

Fig. 6 Numbering of the nodal displacement vector components in the local axis ($\vec{x}$, $\vec{y}$, $\vec{z}$) attached to element e

$$
\begin{aligned}
&L_1^e = 1-\xi, \quad L_2^e = \xi \\
&H_1^e = 1-3\xi^2+2\xi^3, \quad H_2^e = L^e\xi(\xi-1)^2, \\
&H_3^e = 3\xi^2-2\xi^3, \quad H_4^e = L^e\xi^2(\xi-1)
\end{aligned}
\tag{29}
$$

where L^e is the length of the element and $\xi = \frac{x}{L^e}$ is the dimensionless co-ordinate.

The choice of such shape functions makes certain displacement continuity from one element to another. Displacement discretisation is written as

$$
\begin{aligned}
u_x^e &= L_1^e q_1^e + L_2^e q_7^e, \\
u_y^e &= H_1^e q_2^e + H_2^e q_6^e + H_3^e q_8^e + H_4^e q_{12}^e \\
u_z^e &= H_1^e q_3^e - H_2^e q_5^e + H_3^e q_9^e - H_4^e q_{11}^e, \\
\omega^e &= L_1^e q_4^e + L_2^e q_{10}^e
\end{aligned}
\tag{30}
$$

or under the matrix form

$$u^e = N^e q^e \tag{31}$$

Substituting Eq. 30 in Eq. 28 we obtain the generalised strain shape matrix b^e so that

$$e^e(x) = b^e(x)\,q^e \tag{32}$$

with e^e the column vector containing ε^e, K_z^e, K_y^e, K_x^e for element e. Matrix b^e is given by:

$$b^e(x) = \begin{pmatrix} \frac{dL_1^e}{dx} & 0 & 0 & 0 & 0 & 0 & \frac{dL_2^e}{dx} & 0 & 0 & 0 & 0 & 0 \\ 0 & \frac{d^2H_1^e}{dx^2} & 0 & 0 & 0 & \frac{d^2H_2^e}{dx^2} & 0 & \frac{d^2H_3^e}{dx^2} & 0 & 0 & 0 & \frac{d^2H_4^e}{dx^2} \\ 0 & 0 & -\frac{d^2H_1^e}{dx^2} & 0 & \frac{d^2H_2^e}{dx^2} & 0 & 0 & 0 & -\frac{d^2H_3^e}{dx^2} & 0 & \frac{d^2H_4^e}{dx^2} & 0 \\ 0 & 0 & 0 & \frac{dL_1^e}{dx} & 0 & 0 & 0 & 0 & 0 & \frac{dL_2^e}{dx} & 0 & 0 \end{pmatrix} \tag{33}$$

Equation 27 is written in the matrix form

$$\varepsilon^e = G(y,z)\cdot e^e(x) \tag{34}$$

where ε^e is the column vector containing $\varepsilon_{xx}^e, \gamma_{xy}^e, \gamma_{xz}^e$, and matrix G is defined by

$$G(y,z) = \begin{pmatrix} 1 & -y & z & 0 \\ 0 & 0 & 0 & -z \\ 0 & 0 & 0 & y \end{pmatrix} \tag{35}$$

Substituting Eq. 32 in Eq. 34, we obtain strain expressions in terms of nodal displacements:

$$\varepsilon^e = B^e q^e \tag{36}$$

The strain shape matrix B^e due to beam assumptions have the following particular form

$$B^e = G^e(y,z)\,b^e(x) \tag{37}$$

The elementary nodal load vector f^e due to self weight is defined as performing the same mechanical work into nodal displacement q^e as body forces P^e into displacement U^e. This definition is written as

$$\int_{\Omega^e} \left(P_x^e U_x^e + P_y^e U_y^e + P_z^e U_z^e\right) d\Omega = (f^e)^T q^e \tag{38}$$

where Ω^e is the volume of element e.

The beam cross-section area S^e is supposedly small enough to neglect moments of body forces, i.e. using notation in Fig. 5, $\int_{S^e} GM \times P^e dS = 0$. According to Eqs. 26 and 31, f^e is given by

$$f^e = \int_{L^e} (N^e)^T p^e dx \tag{39}$$

where p^e is the 4×1 vector of self-weight distributed density

$$p^e = \begin{pmatrix} \int_{S^e} P_x^e dS & \int_{S^e} P_y^e dS & \int_{S^e} P_z^e dS & 0 \end{pmatrix}^T \tag{40}$$

References

Alméras T, Gril J, Costes E (2002) Bending of apricot tree branches under the weight of axillary growth: test of a mechanical model with experimental data. Trees 16:5–15

Archer RR (1986) Growth stresses and strains in trees. Springer, Berlin Heidelberg New York

Archer RR, Wilson BF (1970) Mechanics of the compression wood response. I. Preliminary analyses. Plant Physiol 46:550–556

Cannell GR, Morgan J, Murray MB (1988) Diameters and dry weights of tree shoots: effects of Young's modulus, taper, deflection and angle. Tree Physiol 4:219–231

Castéra P, Morlier V (1991) Growth patterns and bending mechanics of branches. Trees 5:232–238

Ford ED (1985) Branching, crown structure and the control of timber production. In: Cannell NGR, Jackson JE (eds) Trees as crop plants. Institute of Terrestrial Ecology, Monks Wood, England, pp 228–252

Fournier M, Bordonne PA, Guitard D, Okuyama T (1990) Growth stress patterns in tree stems – a model assuming evolution with the tree age of maturation strains. Wood Sci Technol 24:131–142

Fournier M, Baillères H, Chanson B (1994) Tree biomechanics: growth, cumulative prestresses, and reorientations. Biomimetics 2:229–251

Gillis PP (1973) Theory of growth stresses. Holzforschung 27:197–207

Kubler H (1959) Studien über Wachstumsspannungen des Holzes. Zweite Mitteilung: Die Spannungen in Faserrichtung. Holz Roh Werkst 17:44–54

Mattheck C, Kubler H (1995) Wood – the internal optimization of trees. Springer, Berlin Heidelberg New York

Morgan J, Cannell GR (1988) Support costs of different branch designs: effects of position, number, angle and deflection of laterals. Tree Physiol 4:303–313

Niklas KJ, O'Rourke TD (1982) Growth patterns of plants that maximize vertical growth and minimize internal stresses. Am J Bot 69:1367–1374

Owen DRJ, Hinton E (1980) Finite elements in plasticity – theory and practice. Pineridge, Swansea

Timell TE (1986) Compression wood in gymnosperms. 2. Springer, Berlin Heidelberg New York

Wilson BF, Archer RR (1974) Mechanical aspects of the regulation of branch growth in *Pinus strobus* L. In: Bieleski et al (eds) Mechanisms of regulation of plant growth. The Royal Society of New Zealand, Wellington, pp 631–636

Zienkiewicz OC, Taylor RL (1998) The finite element method, 4th edn, vol 2. Solid and fluid mechanics dynamics and non-linearity. McGraw-Hill, New York